AIAA 2013-2252

On the use of Particle Image Velocimetry to predict trailing edge noise

M.Tuinstra*
National Aerospace Laboratory NLR, Emmeloord, The Netherlands

S. Pröbsting† and F.Scarano‡
Delft University of Technology TU Delft, Delft, The Netherlands

The feasibility of aeroacoustic noise predictions based on Particle Image Velocimetry (PIV) measurements is studied. For this purpose, experiments are conducted on a sharp trailing edge (TE) flow developed along a flat plate at free stream velocity of 15m/s. The acoustic emissions were characterized in the NLR Small Anechoic Wind Tunnel (KAT) by means of microphone measurements. The result is used for benchmarking the PIV based noise predictions. PIV measurements were carried in a low-speed wind tunnel of TU Delft with similar properties to that of the KAT facility. Planar PIV measurements, performed at high spatial resolution, characterize the turbulent properties of the boundary layer travelling across the trailing edge. Time resolved Tomographic PIV measurements are obtained over a *volume* of 19.7mm x 9.1mm x 33.4mm at an acquisition rate of 12kHz. Two different approaches are compared for the prediction of TE noise based on PIV data. The first follows diffraction theory and requires the deduction of the instantaneous surface pressure fluctuations from PIV data. The second one relies on the integral solution of the Lighthill equation obtained through a tailored Green's function for a semi-infinite half plane. This allows to calculate the scattered noise directly from the velocity data. The predictions based on diffraction theory agree well with the measured far field spectrum up to 4kHz. In contrast, the Green's function approach yields a significant and systematic overprediction of approximately 12dB.

I. Introduction

THE European project Advanced Flow Diagnostics for Aeronautical Research (AFDAR) aims at the evaluation and development of state-of-the-art Particle Image Velocimetry (PIV) techniques (www.afdar.eu). The use of PIV for the derivation of pressure has received ample attention in recent years and its feasibility has now been well established[1]. An intuitive extrapolation along this line of work is the use of PIV for the determination of the acoustic emission into the far field.

With the availability of diode-pumped high-speed laser and CMOS cameras, PIV has become accepted and used as a tool for aeroacoustic research[2]. Various researchers[3,4] have applied phase-locked and time-resolved planar PIV for the investigation of the noise sources at a sharp and blunt trailing edge. Lorenzoni et al.[5,6] showed for a rod-airfoil configuration that time-resolved (TR) planar PIV measurements allows the calculation of the hydrodynamic pressure field and the acoustic emission. The tonal noise component, resulting from the impingement of quasi-2D Karman vortices shed from the rod, could be adequately predicted by application of Curle's analogy[7]. The broadband noise prediction showed reasonable agreement with noise measurements, after spanwise coherence length was accounted for. More recently, Violato et al.[8] carried out experiments on a water jet configuration for which time resolved volumetric (4D) PIV was used to evaluate noise emission through the application of Lighthill's acoustic analogy.

* R&D engineer Aeroacoustics, Helicopters and Aeroacoustics department, Marthijn.Tuinstra@nlr.nl
† Research assistant, Aerodynamics section, S.Probsting@tudelft.nl
‡ Head of department Aerodynamics, Wind Energy, Flight performance and Propulsion, Faculty of Aerospace Engineering, F.Scarano@tudelft.nl

The objective of the current work is to assess the feasibility of broadband noise prediction based on PIV in low speed air flows. To achieve this objective, broadband trailing edge (TE) noise emission of a flat plate configuration is considered. An advantage of the flat plate geometry is that analytical approaches are available[9] to predict the noise scatter into the far field. Note that a more complex geometry would require a numerical assessment (e.g. by a Boundary Element Method) which would introduce another element (and potential source of error) in the computational chain. The simple geometry furthermore eases the task of tailoring the Tomographic PIV system to the experiment. Nevertheless, the instantaneous volume flow measurements were restricted to a single side of the trailing edge.

In the present work first trailing edge noise measurements are obtained with a proven methodology[10]. Secondly, time-resolved 3D PIV measurements are achieved using high-speed Tomographic PIV. Finally, the PIV measurements are used as input for acoustic predictions, which are evaluated against the benchmark. For the noise prediction two approaches are followed. One uses Amiet's theory[11] and requires the deduction of the surface pressures from the PIV data. The second approach relies on a tailored Green's function[12] for a semi-infinite half plane to calculate the scattered noise directly from the velocity data. In this respect, well known methods are followed that would normally apply either surface pressure measurements[13] or velocity fields obtained by numerical simulation[14] as input. The significant difference is that now surface pressure spectra and velocity fields obtained through PIV provide the basis for the noise prediction.

II. Experimental apparatus and measurement procedures

A. Acoustic measurements

The Small Anechoic Wind Tunnel (KAT) at NLR is an open circuit, open jet wind tunnel. The test section is surrounded by a 5m x 5m x 3m room, which is completely covered with 0.5m foam wedges, yielding more than 99% absorption above 500 Hz. Two horizontal end-plates (0.90m x 0.70 m) on the upper and lower side of the rectangular 0.38m x 0.51m nozzle provide a semi-open test section for airfoil self-noise measurements (see Figure 1 and Figure 2). To suppress reflections, the end-plates are acoustically lined with a 5.5cm layer of sound absorbing foam covered by a 5% open perforated plate.

The aluminium flat plate has a chord length of 600mm and a span of 510mm, with a thickness of 10mm. It has an elliptical leading edge and a trailing edge with wedge angle of approximately 4.8 degrees. The plate is installed vertically between the end-plates at zero angle of attack. The thickness at the TE is less than 200μm.

The boundary layer on the plate was tripped with a 10 mmwide stripe of carborundum 24 (grain size 0.84mm) over the complete span, yielding homogeneous turbulence characteristics along the span. The trips were applied on both sides of the plate 100mm downstream of the leading edge.

Hot-wire measurements were carried out with a DANTEC StreamLine CTA system. A single wire probe (DANTEC 55P01, 1.25 mm wire length and 5 μm diameter) was used with the wire parallel to the flat plate trailing edge.

The microphone array consisted of 48 LinearX M51 ½-inch microphones mounted in an open grid. The system was designed for maximum side-lobe suppression at frequencies between 1kHz and 20kHz. All microphones, except for two closely spaced microphones at the centre of the array, were equipped with wind screens. To obtain high resolution at low frequencies, the array dimensions needed to be rather large (0.8m x 0.6m). The array was placed outside the tunnel flow at a distance of 0.6m from the tunnel axis. The relatively small distance between the array and the model was chosen to obtain maximum signal-to-noise ratio and resolution. The centre of the array was placed at the same height as the tunnel axis.

B. PIV measurements

Planar and tomographic PIV measurements were carried out in the W-tunnel at the Aerodynamics Laboratories of TU Delft. The facility has a similar layout as the NLR KAT tunnel with an open jet and open-return circuit. It features a square test section of 0.4m x 0.4m with a free stream turbulence level below 0.5% at the exit. Measurements are performed at 15m/s on the flat plate described above.

Three LaVision *HighspeedStar* CMOS cameras (1024x1024 pixels, 12 bits, 20μm pixel size) equipped with Nikkor 105mm prime objectives are arranged as indicated in Figure 3. For the top and bottom cameras, the optical axes deviates from the surface normal by an angle of approximately 30° in the y-z plane and 10° in the x-y plane, while the optical axes of the centre camera includes deviates by angles of 15° and 15°, respectively, such to subtend a solid angle that improves the accuracy of tomographic reconstruction[15]. A numerical aperture of $f_{\#}$=11 provides a sufficient depth of field to maintain all illuminated particles in focus and Scheimpflug adapters correct for the angle

between object and sensor plane. Illumination is provided by a Quantronix *Darwin Duo* Nd:YLF (2x25 mJ at 1kHz) laser and a multi-pass light amplification system maximizes the light intensity in the measurement volume[16]. Figure 4 illustrates the measurement set-up.

Time-resolved sequences of images are recorded at f_s=12kHz. The particle tracers displacement between consecutive images in the free stream is approximately 1.25mm (28 voxels). The particle density is estimated to be of approximately 0.06 particles per pixel (ppp).

LaVision software *Davis* 8 is used for system synchronization and image acquisition. Furthermore, self-calibration[17] is applied, followed by reconstruction with the MART algorithm[18]. The average imaging magnification is M=0.45. The size of discrete voxels used in the reconstruction is is 44.7µm. The data set contains 9,000 vector fields for a measurement of 0.8s.

The sequence of objects is analysed with a volume deformation iterative multigrid technique[19] (VODIM). The high-speed acquisition in single-frame continuous mode allows to strengthen the correlation signal by a short-time sliding-average correlation technique SAC[20] whereby the interrogation kernel encompasses three subsequent objects (two object pairs). Due to the strong shear rate close to the wall, the iterative analysis is stabilized by setting any velocity vector at or below the wall to zero. This approach has been demonstrated to significantly reduce the number of spurious vectors[21]. The interrogation block at the final iteration is performed with a kernel of 28x16x28 voxels and an overlap of 75%.

Table 1: Parameters for tomographic PIV experiment

Parameters	Symbol	Value
Measurement volume size	V	20mm x 9mmx 33mm
Interrogation volume size	δx, δz	1.25mm
	δy	0.72mm
Magnification	M	0.45
Particle displacement	Δx	1.25mm
Acquisition frequency	f	12kHz
Number of samples	N	9,000

Complementary measurements with higher wall-normal resolution are performed with 2C PIV. The field of view is approximately 5.4cm x5.4cm with a plane on the mid span trailing edge. The 5,000 double frame images are acquired at 125Hz with a pulse separation equivalent to a free stream displacement of approximately 10px.They are correlated using LaVision *Davis* with interrogation windows of 0.64mm x 0.64mm (12x12 pixels) and 75% overlap, yielding a vector spacing of 0.16mm.

III. Data acquisition and processing procedures

A. Phased array measurements

The acoustic data from the array microphones were synchronously measured using the VIPER data-acquisition system[22]. The data were acquired with a sample frequency of 30.72kHz for a measurement time of 30s. A 500Hz high-pass filter and 15360Hz low-pass filter were applied to the signal before the AD converter. Before and after the measurements, the sensitivity at 1kHz was checked for all array microphones using a calibrated pistonphone. Frequency-dependent sensitivities of individual microphones were taken from calibration sheets. No corrections were applied for microphone directivity, because this effect is the same for the different configurations and amounts to less than 2 dB for angles up to 45° and frequencies up to 15 kHz. Phase matching of the microphones was checked prior to the measurements using a calibration source at a known position.

The array data were processed using the SOLACAN software[23], which produces acoustic source maps in 1/3-octave bands using conventional beamforming. In this way, noise originating from the model is separated from background noise. To improve the resolution and further suppress background noise from the tunnel, the main diagonal in the cross-power matrix (auto-powers) was discarded. The effect of sound refraction by the tunnel shear layer was corrected using a simplified Amiet method[24], where the shear layer centre was assumed to be at the same y location as the edge of the tunnel nozzle. Furthermore, a spatial window was applied to the microphone signals, in order to correct for the variation in microphone density over the surface of the array. Finally, another spatial window was applied which reduces the effective array aperture with increasing frequency, in order to reduce coherence loss

effects. The array scan plane was placed in the plane of the flat plate. The density of the scan grid was 1 cm in both the streamwise and vertical direction, and the scan levels were normalized to a distance of 0.282 m [$(4\pi)^{-1/2}$], so that for a monopole source the peak level in the source plot corresponds to the Sound Power Level.

To illustrate the expected resolution of the array, Figure 5 shows simulated source maps for an uncorrelated line source at the trailing edge for the present set-up. It can be seen that the resolution increases with frequency, due to the decreasing acoustic wavelength. At high frequencies, spurious sources (or 'side lobes') appear in the maps.

For quantitative comparison of different conditions, the array results were further processed using a power integration method, which produces narrowband and 1/3-octave band spectra for specific source regions. Again the main diagonal in the cross-power matrix was discarded, and spatial windows were applied to the microphone signals to reduce coherence loss effects. Thus, the levels measured by the array represent noise levels radiated in the average direction of the array microphones, including the weighting as a result of the spatial windows. Because the source directivity for trailing edge noise is expected to be the same for all conditions, the comparison of sound levels from different conditions is valid.

The procedure as in Oerlemans[10] was followed to determine trailing edge noise spectra from the integrated spectra. By defining an integration contour around the mid-span area of the model, background noise and possible extraneous noise sources at the model-endplate junctions were suppressed. The mid-span integration area was centred on the trailing edge. The size of the integration area was 0.2m in chordwise direction and 0.1m in spanwise direction, and the scan resolution was 1cm in both the streamwise and vertical direction. Since the integration area 'cuts' through the line source region at the trailing edge, 'leakage' from source regions outside the integration area into the integration contour, and vice versa, will occur. The magnitude of this effect depends on array resolution, and therefore on frequency. To account for this effect, a line source correction was applied to the integrated levels, which was determined from simulations. The resulting spectral levels are Sound Power Levels produced by 10cm of span.

Despite the use of the trailing edge integration contour, for some conditions (plate configuration, tunnel speed, frequency), the trailing edge noise levels were influenced by background noise from the wind tunnel. The tunnel background noise was quantified by performing acoustic measurements without model for all tunnel speeds. In order to allow fast judgment of the validity of the measured levels, background noise was accounted for as follows. If the signal-to-noise ratio (i.e., the difference between the measurement with plate and without plate) is larger than 3dB (10log2), the trailing edge noise level is corrected for background noise on a pressure-squared basis, and the level is assumed to be valid. If the signal-to-noise ratio is smaller than 3dB, no correction is applied and the level represents an upper limit for the actual trailing edge noise level. A valid trailing edge noise level is indicated by a marker in the spectrum.

B. Surface pressure deduction

Recent studies[25,26] have elaborated on the reconstruction of the wall pressure below a turbulent boundary layer from measured time-resolved volumetric velocity field data $\underline{u}(\underline{x},t)$. A recent review of current state-of-the-art is given by van Oudheusden[1]. Methods for derivation of the pressure from velocity field data are based on the momentum equations and reduce for incompressible flow to the following Poisson equation:

$$\nabla^2 p = -\rho \nabla \cdot \left(\frac{D\underline{u}}{Dt} \right) \tag{1}$$

An accurate estimation of the wall pressure fluctuations relies on a robust estimation of the material derivative in equation 2 based on the measured velocity field. Lagrangian methods[27] based on the reconstruction of a particle trajectory reduce the random noise component when compared to Eulerian estimates. For the reconstruction of the particle path the following recurrence relation is used with $i=1\ldots N$, where N denotes the number of steps for the estimation of the derivative:

$$x\left(t_{\pm i}\right) = \pm u\left(x\left(t_{\pm(i-1)}\right), t_{\pm(i-1)}\right)\Delta t + x\left(t_{\pm(i-1)}\right) \tag{2}$$

The material derivative is then estimated by the difference of the particle velocity at the end points of the trajectory:

$$\frac{D\underline{u}}{Dt} \approx \frac{u(x(t_{+N}),t_{+N}) - u(x(t_{-N}),t_{-N})}{2N\Delta t} \tag{3}$$

The components of the pressure gradient normal to the boundary faces are derived based on the momentum and applied everywhere but at the face closest to the free stream (Neumann boundary condition). At the remaining face an estimation of the fluctuating pressure is imposed (Dirichlet boundary condition) based on a Reynolds decomposition of the flow field and convection corrected Bernoulli equation, as suggested by de Kat[28]:

$$p' = -\frac{1}{2}\rho(u' \cdot u') \tag{4}$$

Close to the wall the random noise component of the velocity field measurements increases due to a higher velocity gradient and overlap of the interrogation window with the wall. Therefore the closest point to the wall where the velocity data is considered for integration is at *y=0.53mm*. The corresponding approximation in terms of pressure is that the contribution of $\delta p/\delta y$ is negligible between this height and the wall. It was verified that this hypothesis does not introduce significant distortion in the results making use of DNS data[25]. The overall methodology has been applied for turbulent boundary layers before[25,26], where wall pressure fluctuations have been compared to direct measurements by pinhole mounted microphones with good agreement.

The Poisson equation is discretized based on a second order central finite difference method and the resulting system of equations is solved iteratively by preconditioned GMRES (generalized minimum residual algorithm). Figure 6a shows a comparison of the estimated wall pressure spectra at the trailing edge for stencils of different length (*N=3,4,5*). The use of a larger stencil tends to reduce the random noise component as is seen in Figure 6a. The acoustic estimations in the remainder of this study are based on the results obtained with *N=5*. The resulting trace of the pressure fluctuations along the span at the location of the trailing edge is shown in Figure 6b.

In principle, the spanwise coherence length of the pressure fluctuations can be determined based on the reconstructed pressure field. In case of limited spatial resolution a semi-empirical model originally proposed by Corcos[29] is an appropriate alternative, which will also be considered in this work (α=0.48):

$$l_z(\omega) \approx \frac{U_c}{\alpha\omega} \tag{5}$$

An estimation of the convection velocity is obtained through a cross-correlation analysis of two points separated by a distance Δx. The maximum of the correlation signal at t_{max} gives an estimate of the convection velocity with $U_c=\Delta x/t_{max}=0.73$. Note that the exact value of the constants is not of crucial importance for an estimation of the far field noise due to the collapse of the decibel scale.

IV. Noise characteristics

A. Source maps

The acoustic source maps for the flat plate with carborundum trip at different tunnel speeds are shown in Figure 7 to Figure 10. The dB scale is adjusted for each map and the range is always 12 dB. The black line indicates the position of the trailing edge and flow is from left to right. Similar to the simulations (Figure 5), the resolution increases with increasing frequency. The appearance of the line sources in Figure 8 is very similar to the simulations. For increasing tunnel speed the line sources appear at higher frequencies, which is typical for trailing edge noise. At high tunnel speeds, tunnel noise is dominant for the low frequencies. The reason for the increased levels above and below the tunnel axis at 15m/s between 1.6kHz and 2.5kHz (Figure 7) is not known. This phenomenon was repeatable and was also visible at 20m/s.

B. Effect of tunnel speed

The effect of tunnel speed on the trailing edge noise is shown in Figure 11. As expected, both the levels and the dominant frequencies increase with increasing tunnel speed. According to aeroacoustics theory[30], the sound levels are expected to scale according to $p^2 \sim U_t^5$, with p the acoustic pressure and U_t the tunnel speed. The dominant frequencies are expected to be proportional to U_t. The result of applying this scaling (normalized sound levels versus Strouhal number with unity length scale) is shown in Figure 12. It can be seen that the spectra for the different tunnel speeds collapse within about 5 dB.

A better data collapse may be obtained by using the boundary layer displacement thickness at the trailing edge length to scale the levels and frequencies[30]. On the basis of the HWA results, the displacement thickness was found to scale with Reynolds number as follows: $\delta^* \approx 0.04 \cdot C \cdot \mathrm{Re}^{-0.12}$. The result is shown in Figure 13. It appears that the data collapse hardly improves with respect to the previous figure. Estimating the displacement thickness using the theoretical relation[31] $\delta^* \approx 0.05 \cdot C \cdot \mathrm{Re}^{-0.2}$ did not improve the data collapse either (not shown in here). The best data collapse is obtained by scaling the levels using a speed exponent of 4.5 instead of the theoretical value of 5 (Figure 14). Previous studies on trailing edge noise[10] and slat noise[32,33], which may be regarded as a TE noise mechanism, also showed that scaling with an exponent of 4.5 yields the best data collapse. This slightly reduced exponent may be physical or may be due to coherence loss, which may slightly reduce the integrated spectral levels at high speeds and frequencies, despite the use of an integration contour.

C. Comparison with literature data

Although there is an abundance of work reported on airfoil trailing edge noise, studies dealing with flat plate trailing edge noise are less common. A significant body of work is that of Herr[34,35,36], who used flat plate configurations to study trailing edge noise and means to reduce it. TE noise spectra for a 0.8m flat plat at U_t=40m/s, 50m/s and 60m/s were taken from Herr[35], Figure 4a. The spectra were rescaled using $U^{4.5}$ and δ^* and compared with the NLR data (s_0=10cm) acquired for the carborundum trip (Figure 15). The current data was expressed in SPL by:

$$SPL_{norm} = PWL_{norm} - 10\log 4\pi r^2 + 10\log\frac{s}{s_0} \tag{6}$$

to match the Herr experiment (r=1.15m, s=0.8m). A generic spectrum shape for flat plate trailing edge noise is obtained by a regression fit and also plotted in Figure 15. The data is split in three regions, for which we obtain:

$$PWL_{norm} = SPL_{norm} + 10\log 4\pi r^2 - 10\log\frac{s}{s_0} = \begin{cases} 0.11\ \mathrm{logSt} + 5.2 & \text{for} \quad \mathrm{St}<0.1 \\ -9.1\mathrm{logSt} - 4.0 & \text{for } 0.1<\mathrm{St}<0.53 \\ -188.9\ \ \mathrm{logSt} - 52.9 & \text{for} \quad \mathrm{St}>0.53 \end{cases} \tag{7}$$

Firstly, it is noted that also for the Herr experiment a better collapse of the spectra is obtained when normalizing with $U^{4.5}$. Comparing the two datasets, good agreement is found for St>0.1 showing the same decay with Strouhal number. For St<0.1 the present data shows an approximately constant level whereas Herr reports a continuous increase. In the same figure a predicted[30] noise spectrum for a NACA0012 airfoil at 40m/s is plotted (as shown in Herr[35]), which does not to collapse with the flat plate TE spectra. Since the geometry is not that different, the explanation must be sought in the flow characteristics. The spectrum obtained from the current data flattens out in the same Strouhal range at which the NACA0012 spectrum attains its maximum. It is difficult though to identify where the maximum occurs exactly.

V. Flow characteristics

A. Average flow field

Figure 16 shows a contour plot of the normalized average u-component for the 2C PIV and Tomographic PIV measurement (boxed area). An excellent agreement is found between the two measurements. Only in the upper right corner of Tomographic PIV measurement area a degradation of the measurement quality is noticed. In this area the signal-to-noise ratio is low as a result of reduced illumination intensity at the border of the measurement volume. When velocity profiles are examined (Figure 17) it confirms the above, displaying excellent agreement. At 5mm behind the trailing edge HWA measurements were obtained for the KAT experiment which are also plotted in Figure 17. Also in this case a good agreement is found, showing a minimum wake velocity of $0.42U_t$ and near identical profile shape.

B. Turbulence intensity

A contour plot of turbulence intensity is given by Figure 18. Though demonstrating a similarity, the agreement between Tomographic PIV and 2C-PIV is not as convincing as for the average velocity. Figure 19 shows the turbulence intensity profiles at several streamwise positions. At (x=0mm) and upstream (x=-5mm, x=-10mm) of the trailing edge a similar profile shape is found. However, the peak intensity at the wall is not captured fully by the Tomographic PIV measurement and further away from the wall 0.5% higher turbulence levels are found. The drop in peak intensity is ascribed to insuficient spatial resolution, which is twice lower than 2C PIV. This results in a spatial averaging of small scale turbulent structures which predominantly exist at the near-wall-region. The reason for slight increase in turbulence levels for the outer part may be ascribed to the effect of ghost particles prevailing in this region where the illumination intensity is lower. The observed behaviour is consistent with the effect of ghost particles velocity as reported in a study given by Elsinga et al.[37].

For the near trailing edge wake (x=5mm) the results of the Hot-wire experiments in the KAT facility are plotted as well. The peak intensity occurs at the same wake location and the levels for the Hot-wire and 2C-PIV experiment are in agreement (~$0.1U_t$). The profile shape is similar, although the Hot-wire measurements show about 1% higher turbulence intensity levels. Inspection of the Hot-wire autospectrum at y=25mm showed increased turbulence levels for the low frequency range (f~10Hz). This phenomenon is typically related to the column instability of the tunnel jet and not to the flat plate boundary layer. The occurrence and intensity is facility dependent and apparently weaker for the W-Tunnel. From the average velocity and turbulence intensity analysis, it can be concluded that the experiment reproduces well between facilities.

C. Turbulence spectra

Spectral analysis of the acquired Tomographic PIV measurements was carried out and compared to the Hot-wire spectra (Figure 20). This was done for three y-locations: at maximum turbulence intensity (y=0.7mm), at the middle of the volume (y=2.6mm) and at the upper part of the volume (y=6.6mm). At all three locations a good correspondence is obtained for the lower frequencies.

Closest to the wake centre (y=0.7mm), appreciable discrepancies are found for 500Hz and above. Moving to the outer part of the wake the results progressively improve. As was stated in section B this is likely due to insuficient spatial resolution. The interrogation volume size is 1.2mm x 1.2mm x 0.7mm. If we assume roughly six points are required to resolve a turbulent structure in space and a convection speed of $0.6U_t$, measurements up to ~1200Hz should be fully resolved. Therefore, with respect to the acquisition rate of 12kHz the spatial resolution is an order of magnitude too small to capture the correct amplitude.

Since PIV is a digital measurement technique, analogue filtering of the signal is not possible and aliasing could potentially be an issue. Although the PIV spectra do show a minor increase of spectral energy content at the end of the frequency range that could be related to aliasing, the impact is negligible.

VI. Noise prediction

Since the measurement volume is restricted to a single side of the plate, the analysis requires the assumption that the boundary layer on the opposite side represents an uncorrelated source region of equal strength (+3dB). The predictions consider a span equivalent to $s_0=10cm$ and an observer located at a distance of $R=0.282m$ to allow direct comparison with the acoustic measurements. The acoustic measurements were obtained using a microphone array and therefore correspond to an average over the area of the array. To take into account the influence of the spatial averaging due to directivity of the source, the average noise prediction over the area of the array is considered (although the effect was found to be small).

Two approaches were considered of which the first relies on diffraction theory. The formulation applied in this study follows that of Roger and Moreau[38,39]. Leading edge back-scattering is not considered for the results presented here. In this case the surface pressure spectrum upstream of the trailing edge serves as input, which is obtained from the flow volume measurements through a pressure deduction procedure as is described in section III.B. The scattered disturbance pressure, in response to the measured incident pressure disturbance, is obtained by solving a Schwarzschild problem, imposing a Kutta condition at the trailing edge. Subsequently, this can be related to the acoustic far-field pressure by the radiation integral. The farfield powerspectrum is then given by:

$$S_{pp}\left(\bar{x},\omega\right)=\left(\frac{k\,c\,y}{4\pi S_0^2}\right)^2 2L\left|\mathscr{L}\right|^2\phi_{pp}\,l_z \tag{8}$$

where S_0 is the convection-corrected observer distance, k is the acoustic wavenumber, c the airfoil length and L the span length. $\mathscr{L}$ represents the acoustic transfer function and defines the scatter response to an the incoming pressure disturbance specified by the wall pressure spectrum ϕ_{pp}, and the spanwise correlation length l_z. For details refer to ref.[11,38,39].

The second approach relies on the integral solution to the Lighthill equation derived by Ffowcs-Williams and Hall[12] to obtain the acoustic pressure. It is obtained by applying the tailored thin half-plane Green's function and given by:

$$-4\pi\,\hat{p}\left(r,\theta,\zeta;k\right)=k^2\,\frac{2e^{i\frac{\pi}{4}}}{\sqrt{\pi}}\sin\left(\frac{\theta}{2}\right)\int_{V_0}\left\{\rho\left(v_r^2-v_\theta^2\right)\sin\left(\frac{\theta_0}{2}\right)+2\rho v_r v_\theta\cos\left(\frac{\theta_0}{2}\right)\right\}\frac{\sin\phi^{1/2}}{\left(2kr_0\right)^{3/2}}\frac{e^{-ikR}}{R}dV_0 \tag{9}$$

In this the carrot indicates a temporal Fourier transform, k is the acoustic wavenumber and v_r and v_θ are the velocity components defined in cylindrical coordinates. For this approach the measured velocity fields directly serve as input to the volume integral over the source region (V_0), representing quadrupole sound sources. The coordinate system definition is given in Figure 21.

Figure 22 shows the noise predictions compared to the measured sound power levels. The results based on diffraction theory match very well with the measured noise levels. Until 1.6Khz predicted levels are within 2dB of the measured levels. For 2kHz and above the spectrum shape and in particular the sudden drop in acoustic levels is not well predicted. This could be the result of insufficient spatial resolution of the PIV measurement, needed to accurately capture the associated turbulence scales. To deal with this issue, a simple empirical model[29] for span coherence of surface pressure was applied as well. Although a minor improvement was obtained for the high frequencies, the trend as shown by the measurements was not recovered.

In the same figure the results for the Ffowcs-Williams and Hall approach are presented as well. Although the

predicted spectral shape is very similar to that obtained by diffraction theory the obtained levels are approximately 12dB higher. A possible answer to why this approach performs worse than diffraction theory is found in a discussion by Blake[40] on the implication of imposing a full Kutta condition at the TE to the noise scattering problem.

The Kutta condition models the viscous reponse to an incoming disturbance in the vicinity of the trailing edge in potential flow theory. If this reponse is in fact of relevance that would imply that the flow measurements should be obtained all around the trailing edge to apply the Ffowcs-Williams and Hall approach succesfully. A simplified consideration by Howe[41] of the noise radiated for an infinite long vortex filament with axis parallel to the trailing edge as it passes the trailing edge shows that the noise emission significantly reduces (~9dB) due to the application of the Kutta condition. Diffraction theory is less susceptible for this since a Kutta condition is explicitly imposed, whereas for the Lighthill solution it has to follow implicitly from the flow measurements in the vicinity of the trailing edge. It is hypothesized that the truncation of the flow domain at y=0 or the limited spatial resolution in the direct vicinity of the trailing edge could be the cause of such overestimation of the noise levels. These hypotheses require further scrutiny and are currently being investigated.

VII. Conclusions

The presented work shows that broadband noise prediction based on volumetric PIV measurements is possible for the elementary case of flat plate trailing edge noise.

An acoustic benchmark was obtained for a flat plate configuration for comparison with PIV based noise predictions. Extraneous noise sources were filtered by use of a phased array. Normalization with $U^{4.5}$ gave a good collapse of the spectra for the measured velocity range. Comparison with literature showed a good agreement.

Volumetric, time resolved flow measurements were carried out at the trailing edge of a flat plate by use of Tomographic PIV. The measurement quality was evaluated against Hot-wire measurements and 2C PIV. The average velocity shows good agreement with both 2C PIV and Hot-wire measurements. The measurements agree to a lower degree for the fluctuating part of the velocity with turbulence peaks damped in the tomographic data and with some evidence of ghost particles affecting the wall-normal distribution of turbulent fluctuations.

PIV based acoustic predictions were carried out based on diffraction theory and an integral solution to the Lighthill equation. The predictions based on diffraction theory showed good agreement with experimental results over a wide range of relevant frequencies. The decline in sound pressure level at higher frequencies however, could not be predicted adequately, which is ascribed to insufficient spatial resolution of the velocity measurements or other unknown extraneous noise sources. The integral solution to the Lighthill equation showed an overprediction of noise levels of approximately 12dB. Truncation of the flow domain at y=0 and insufficient information on the flow in the direct vicinity of the trailing edge was identified as a possible cause for such overestimation. Refraction theory is thought to be less susceptible to this type of error since the eddy-edge interaction is explicitly modelled by imposing a full Kutta condition at the trailing edge.

Acknowledgments

This research is supported by the European Community's Seventh Framework Programme (FP7/2007-2013) under the AFDAR project (Advanced Flow Diagnostics for Aeronautical Research). Grant agreement No.265695.

References

[1] B.W. van Oudheusden, *"PIV based pressure measurement"*, Measurement science & technology, vol. 24, issue 3, 2013

[2] S. C. Morris, "*Shear-Layer Instabilities: Particle Image Velocimetry Measurements and Implications for Acoustics*", Ann. Rev. Fluid. Mech., 43(1), 529–550. doi:10.1146/annurev-fluid-122109-160742, 2011

[3] A. Schröder, M. Herr, T. Lauke and U. Dierksheide, "*Measurements of Trailing-Edge-Noise Sources by means of Time-Resolved PIV*" 6th International Symposium on Particle Image Velocimetry California USA, Vol. 2, pp. 1–8, 2005

[4] D. W. Shannon and S.C. Morris, "*Experimental investigation of a blunt trailing edge flow field with application to sound generation*", Exp. in Fluids, 41(5), 777–788. doi:10.1007/s00348-006-0200-3, 2006

[5] V. Lorenzoni, M. Tuinstra, P. Moore and F. Scarano, *"Aeroacoustic analysis of a rod-airfoil flow by means of time-resolved PIV"*, AIAA-2009-3298, 2009

[6] V. Lorenzoni, F. Scarano and M. Tuinstra, *"On the Use of Time-Resolved Particle Image Velocimetry for the Investigation of Rod-Airfoil Aeroacoustics",* Journal of Sound and Vibration, http://dx.doi.org/10.1016/ j.jsv.2012.05.034, 2012

[7] N. Curle, *"The influence of solid boundaries upon aerodynamic sound"*, Proc. Roy. Soc. Lon., Vol. A 211, 1952, pp.564-587

[8] D.Violato; F.Scarano, *"Three-dimensional vortex analysis and aeroacoustic source characterization of jet core breakdown*", Physics of fluids, Vol. 25, Issue 1, 2013

[9] M.S. Howe, *"A review of theory of trailing edge noise*", Journal of sound and vibration, 61, 437-465, 1978

[10] S. Oerlemans and P. Migliore, *"Aeroacoustic wind tunnel tests of wind turbine airfoils"*, AIAA 2004-3042, 2004

[11] R. Amiet, *"Noise due to turbulent flow past a trailing edge"*, Journal of Sound and Vibration, 47(3), 387–393, 1976.

[12] J.E. Ffowcs Williams and L.H. Hall, *"Aerodynamic sound generation by turbulent flow in the vicinity of a scattering half plane"*, Journal of fluid mechanics, vol.40, no.4, 1970, pp657-670

[13] T.F. Brooks and T.H. Hodgson, "*Trailing edge noise prediction from measured surface pressures"*, Journal of sound and vibration, 78(1), 69-117, 1981

[14] J.Christophe, *"Application of Hybrid Methods to High Frequency Aeroacoustics"*, PhD thesis, 2011

[15] F. Scarano, *"Tomographic PIV: principles and practice"*, Measurement science & technology, vol. 24, issue 1, 2013

[16] S. Ghaemi, and F. Scarano, *"Multi-pass light amplification for tomographic particle image velocimetry applications"*, Measurement Science and Technology, 21(12), 127002, 2010.

[17] B. Wieneke, *"Volume self-calibration for 3D particle image velocimetry"*, Exp. in Fluids, 45(4), 549–556, 2008.

[18] G. T. Herman and A. Lent, *"Iterative reconstruction algorithms"*, Computers in Biology and Medicine, 6, 273–294, 1976

[19] F. Scarano and C. Poelma, *"Three-dimensional vorticity patterns of cylinder wakes"*, Exp. in Fluids, 47(1), 69–83, 2009.

[20] F. Scarano, *"Tomographic PIV: principles and practice"*, Meas. Sci. Technol., 24, 2012

[21] R. Theunissen, F. Scarano and M. L. Riethmuller, *"On improvement of PIV image interrogation near stationary interfaces"*, Exp. Fluids. 45, 557-572, 2008

[22] H. Holthusen and H. Smit, "*A new data-acquisition system for microphone array measurements in wind tunnels"*, AIAA paper 2001-2169, 2001

[23] P. Sijtsma, "*Users guides of acoustic array data processing software - Extended issue; version 7.0"*, NLR-TR-2009-528, 2009

[24] R.K. Amiet, "*Refraction of sound by a shear layer"*, Journal of Sound and Vibration, Vol. 58, No. 2, pp 467-482, 1978

[25] S. Pröbsting, F. Scarano, M. Bernardini and S. Pirozzoli, *"A comparative study of turbulent boundary layer wall pressure fluctuations obtained from high-speed tomographic PIV and DNS",* 16th Int Symp on Appl of Laser Tech to Fluid Mech, Lisbon, 2012

[26] S. Ghaemi, D. Ragni and F. Scarano, *"PIV-based pressure fluctuations in the turbulent boundary layer"*, Experiments in Fluids, 53:6, pp. 1823-1840, 2010

[27] D. Violato, P. Moore and F. Scarano, *"Lagrangian and Eulerian pressure field evaluation of rod-airfoil flow from time-resolved tomographic PIV"*, Experiments in Fluids, 50(4), 1057–1070. doi:10.1007/s00348-010-1011-0, 2010

[28] R. de Kat, "*Instantaneous planar pressure determination from particle image velocimetry",* PhD thesis. Delft University of Technology, 2012

[29] G. M. Corcos, *"The structure of the turbulent pressure field in boundary-layer flows"*, J. Fluid Mech., *18*, 353–378, 1963

[30] T.F. Brooks, D.S. Pope and M.A. Marcolini, "*Airfoil self-noise and prediction"*, NASA Reference Publication 1218, 1989.

[31] H. Schlichting, *"Boundary-Layer theory*", McGraw-Hill, 1979.

[32] M. Pott-Pollenske, W. Dobrzynski, H. Buchholz, B. Gehlar and F. Walle, *"Validation of a semiemperical airframe noise prediction method through dedicated A319 flyover noise measurements"*, AIAA 2002-2470, 2002

[33] M. Pott-Pollenske, J. Alvarez-Gonzales and W. Dobrzynski, *"Effect of slat gap on farfield radiated noise and correlation with local flow characteristics"*, AIAA 2003-3228, 2003

[34] M. Herr and W. Dobrzynski, *"Experimental Investigations in low noise trailing edge design"*, AIAA 2004-2804, 2004

[35] M. Herr, *"A noise reduction study on flow-permeable trailing-edges"*, DLR electronic library, 2007

[36] M. Herr, *"Trailing-edge noise data quality assessment for CAA validation"*, AIAA 2010-3877

[37] G.E. Elsinga, J.Westerweel, F.Scarano and M.Novara, "*On the velocity of ghost particles and the bias errors in Tomographic-PIV*", Exp. Fluids, 50, 825-838, 2011

[38] M. Roger and S. Moreau, *"Extensions and limitations of analytical airfoil broadband noise models"*, International Journal of Aeroacoustics, 9(3), 273–306, 2010.

[39] M. Roger, S. Moreau, *"Back-scattering correction and further extensions of Amiet's trailing-edge noise model",* Part 1: theory, Journal of Sound and Vibration 286 (2005) 477–506.

[40] W.K. Blake, *"Mehanics of flow induced sound and vibration"*, Vol.II, p.732-735, 1986

[41] M.S. Howe, *"The influence of vortex shedding on the generation of sound by convected turbulence"*, J. Fluid Mech., 76, p711-740, 1976

Figures

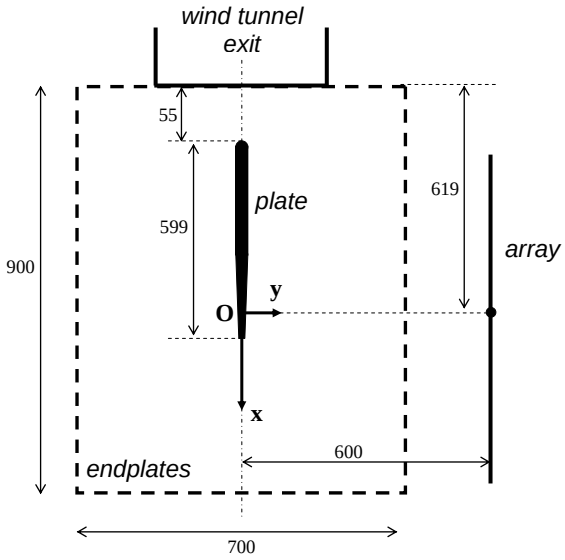

Figure 1. Top view of KAT set-up for trailing edge noise measurements. The microphone array was located on the +y side of the model. The origin of the coordinate system is on the tunnel axis, aligned with the array center. Dimensions in mm (not to scale).

Figure 2. KAT set-up with microphone array and flat plate vertically mounted between the lined endplates.

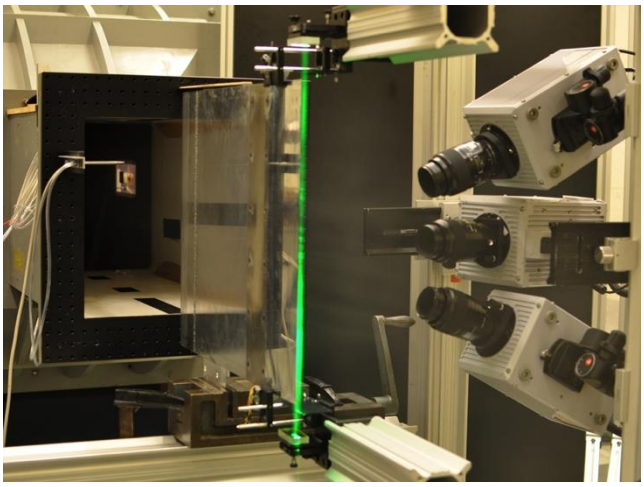

Figure 3. Photograph showing set-up for tomographic PIV experiment in the W-Tunnel.

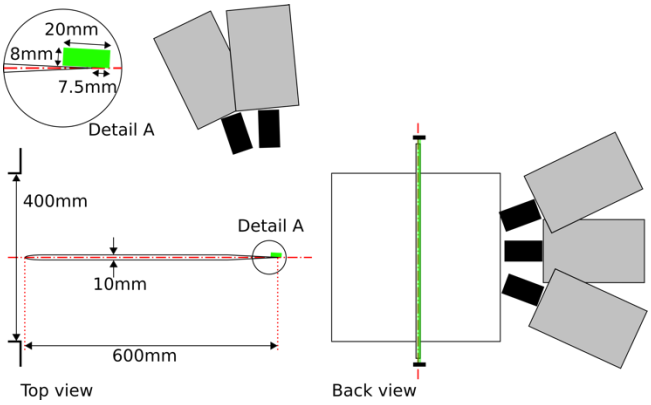

Figure 4. Set-up for tomographic PIV experiment including arrangement of flat plate, multi-pass system for illumination and cameras.

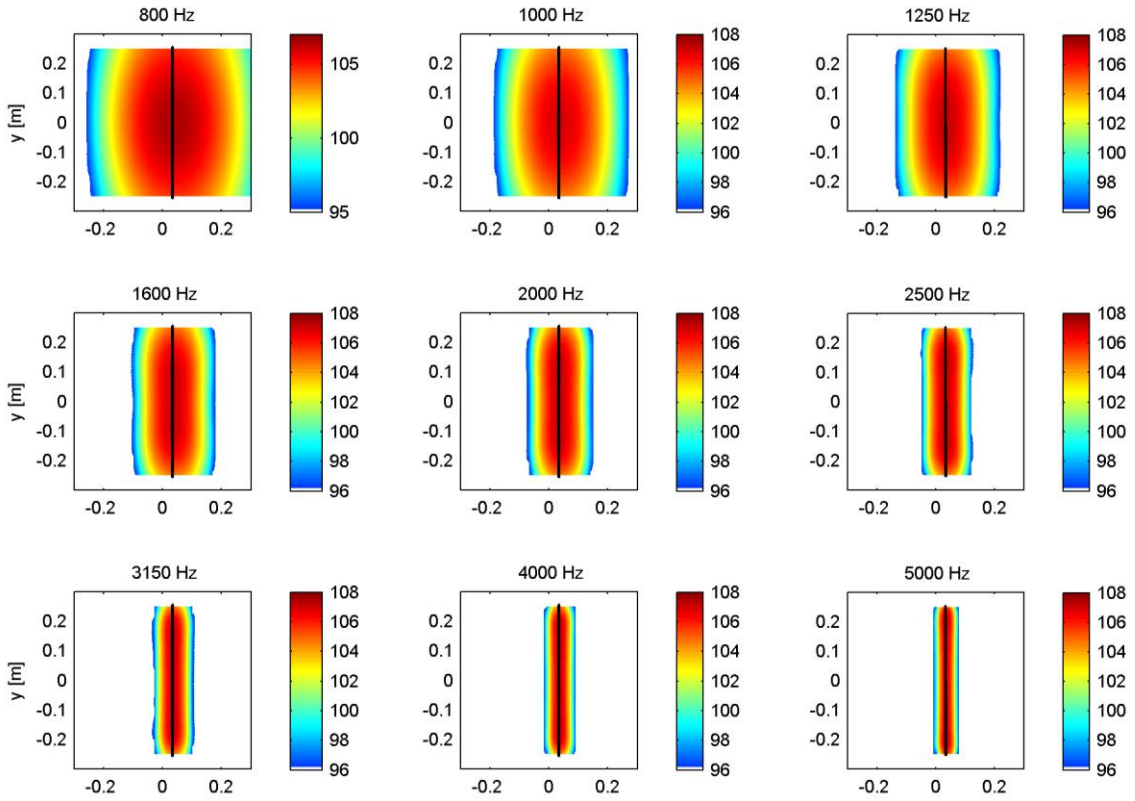

Figure 5. Simulated source maps for an uncorrelated line source (white noise) at the trailing edge. Flow is from left to right and the range of the colour scale is 12 dB. The black line indicates the position of the trailing edge.

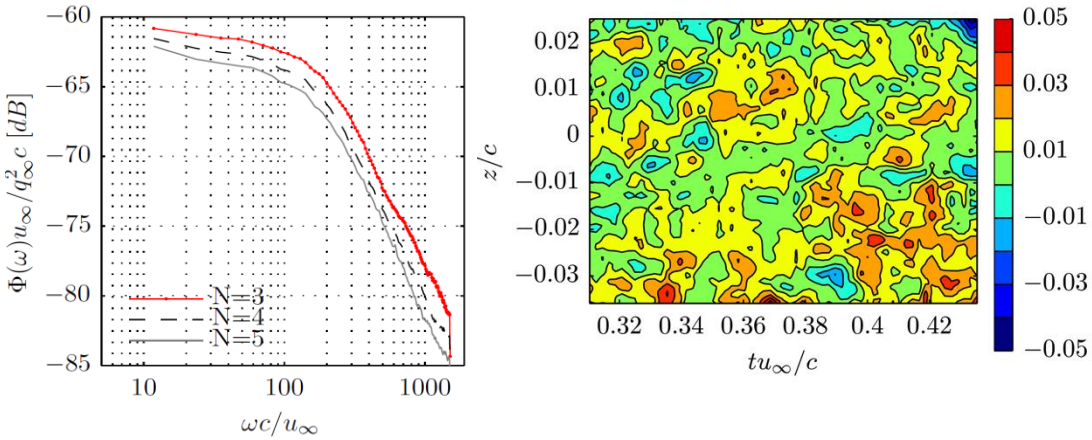

a) b)

Figure 6. Comparison of estimated wall pressure spectra at trailing edge for different stencils (a) and trace of pressure fluctuations (p'/q_∞) at trailing edge for N=5.

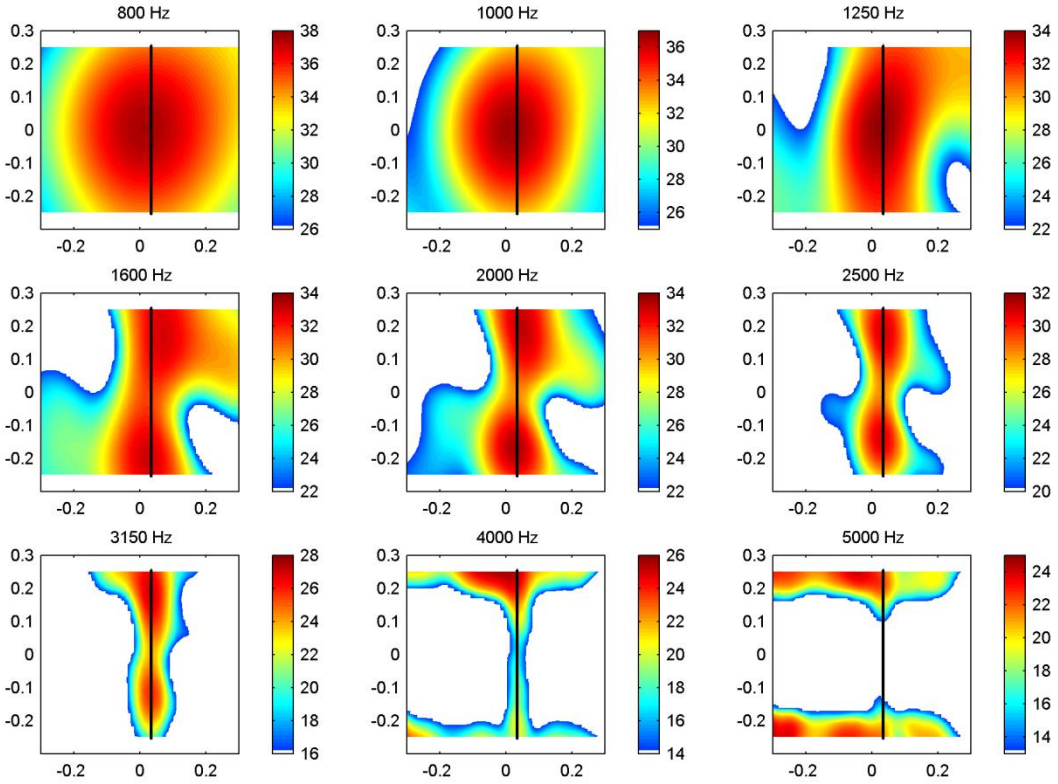

Figure 7. Acoustic source maps for flat plate with carborundum trip at 15 m/s.

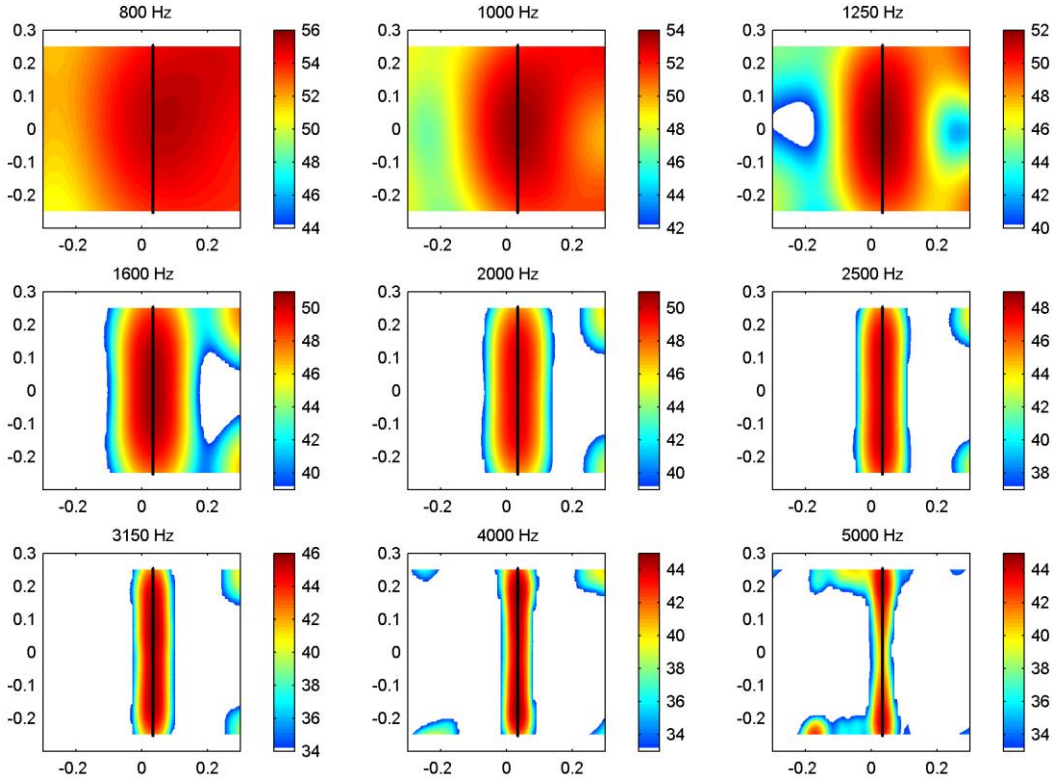

Figure 8. Acoustic source maps for flat plate with carborundum trip at 35 m/s.

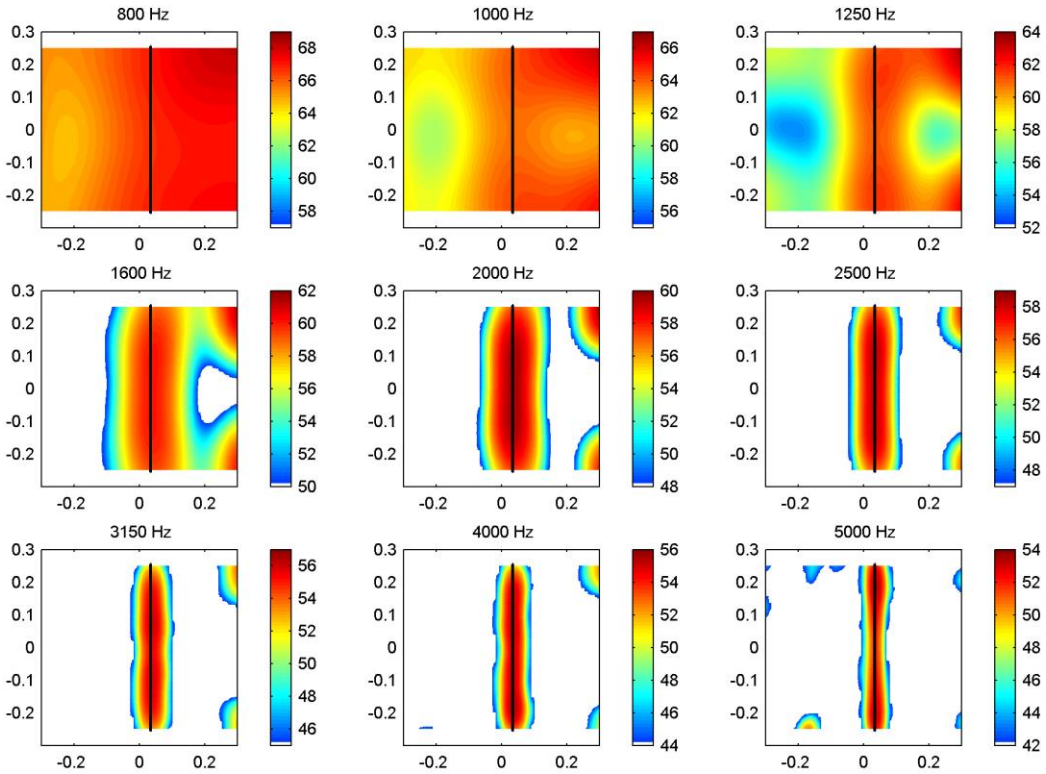

Figure 9. Acoustic source maps for flat plate with carborundum trip at 55 m/s.

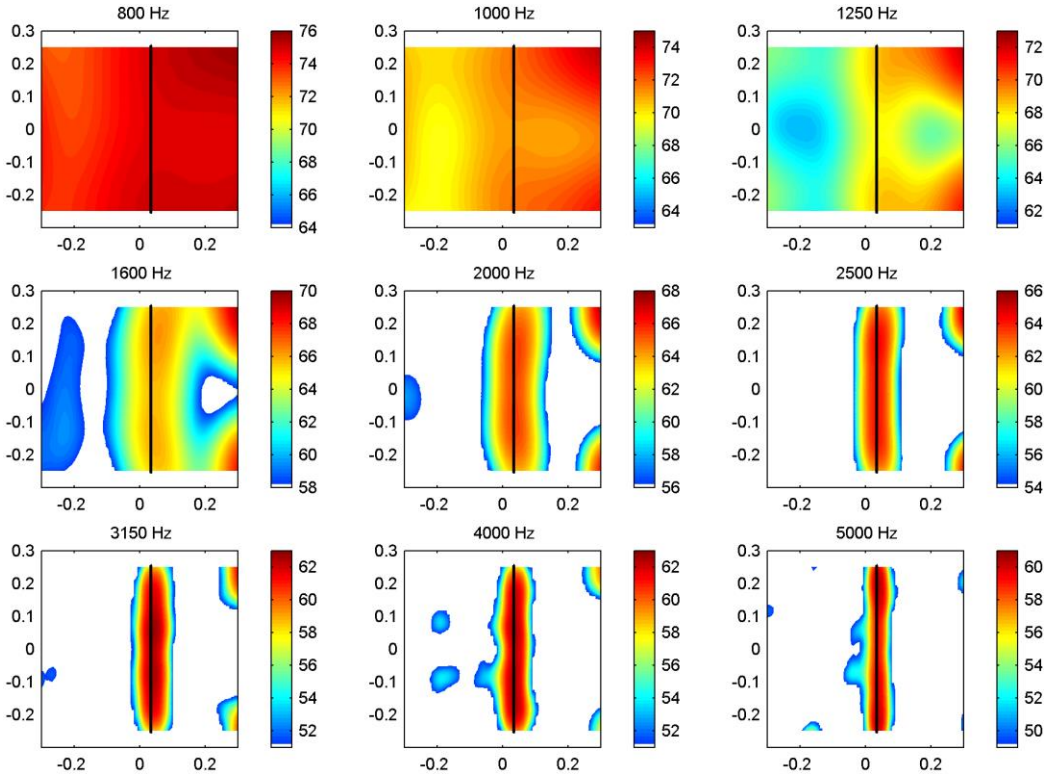

Figure 10. Acoustic source maps for flat plate with carborundum trip at 75 m/s.

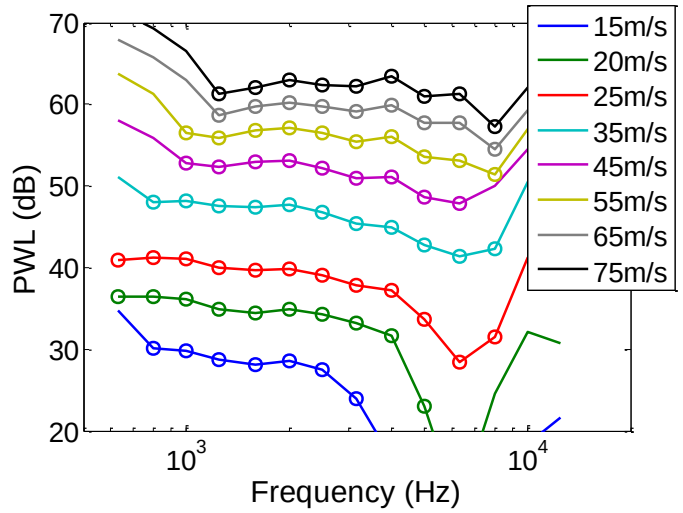

Figure 11. Trailing edge noise spectra as a function of tunnel speed.

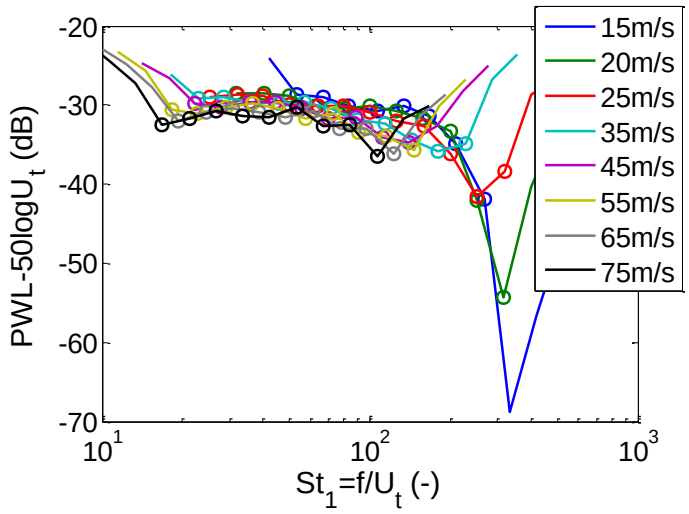

Figure 12. Normalized (unity length scale) trailing edge noise spectra as a function of tunnel speed.

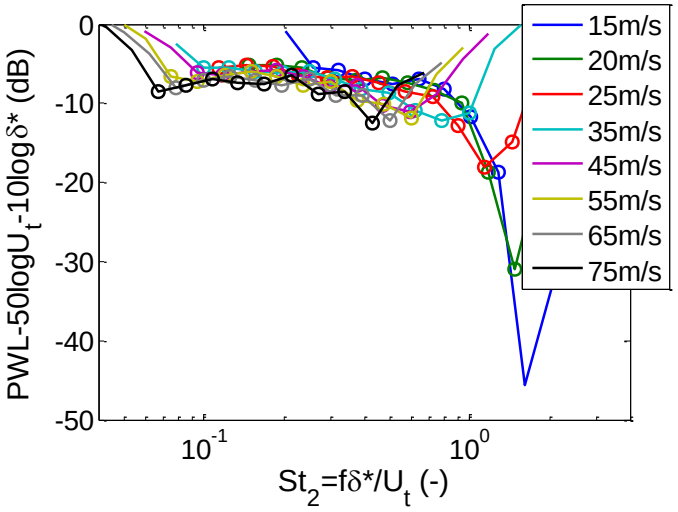

Figure 13. Normalized (scaled with displacement thickness) trailing edge noise spectra as a function of tunnel speed .

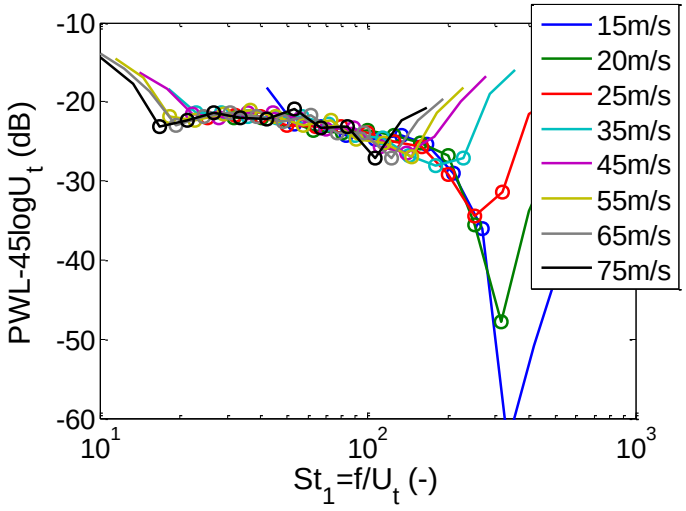

Figure 14. Normalized trailing edge noise spectra (using a speed power of 4.5 instead of 5) as a function of tunnel speed.

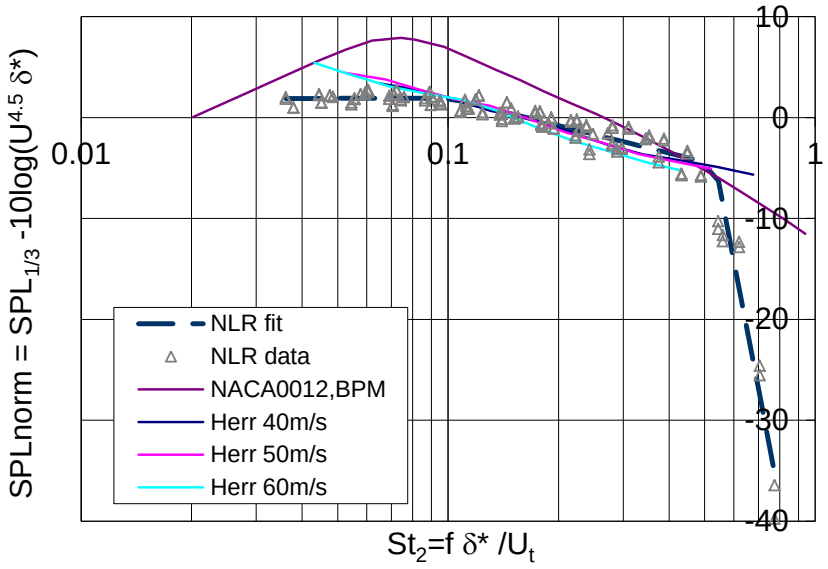

Figure 15. Normalized TE spectra, comparison of data acquired Herr, NACA0012 BPM[30] prediction and NLR data (U_t=15m/s, 20m/s, 25m/s, 35m/s, 45m/s, 55m/s, 65m/s and 75m/s).

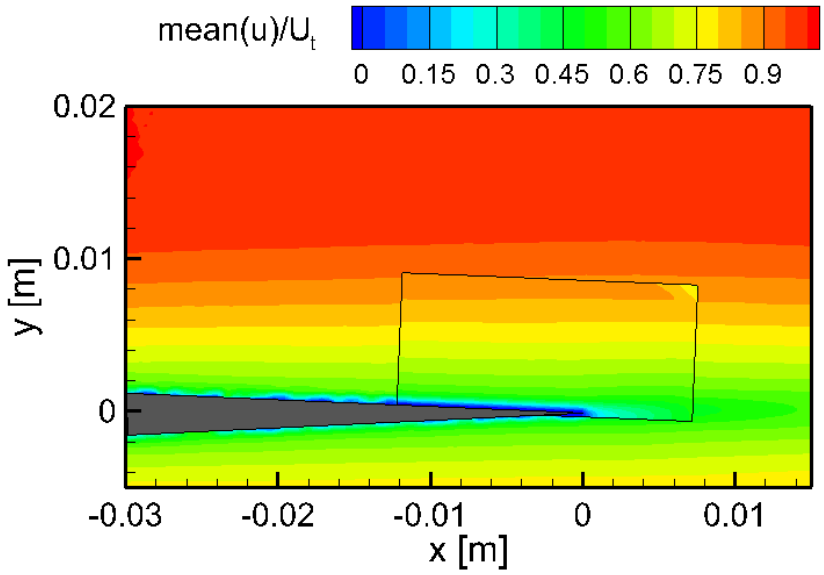

Figure 16. Contour plot of the average u-component, results in the boxed area were acquired by tomographic PIV.

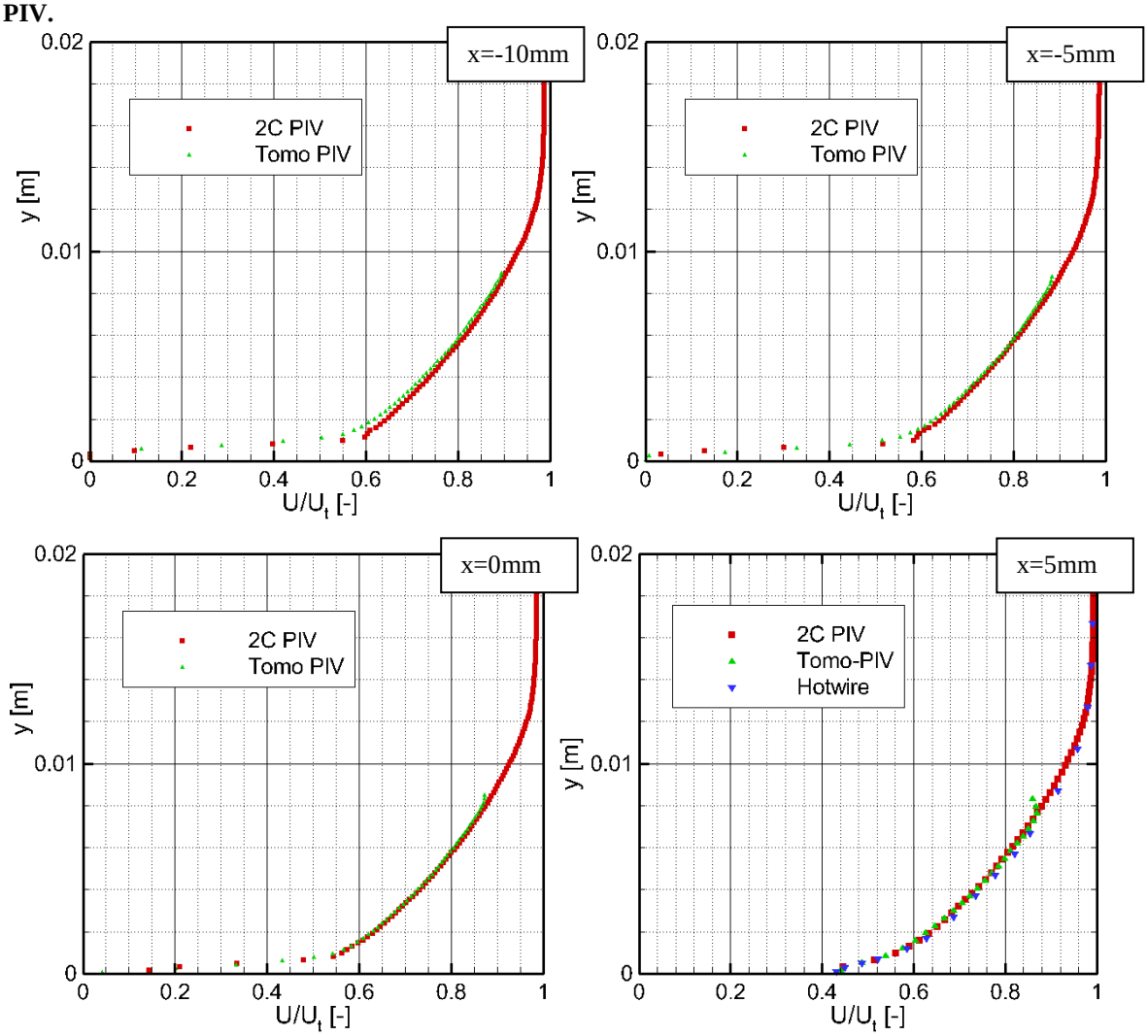

Figure 17. Velocity profiles normalized with tunnel velocity U_t at x=-10mm, -5mm, 0mm and 5mm

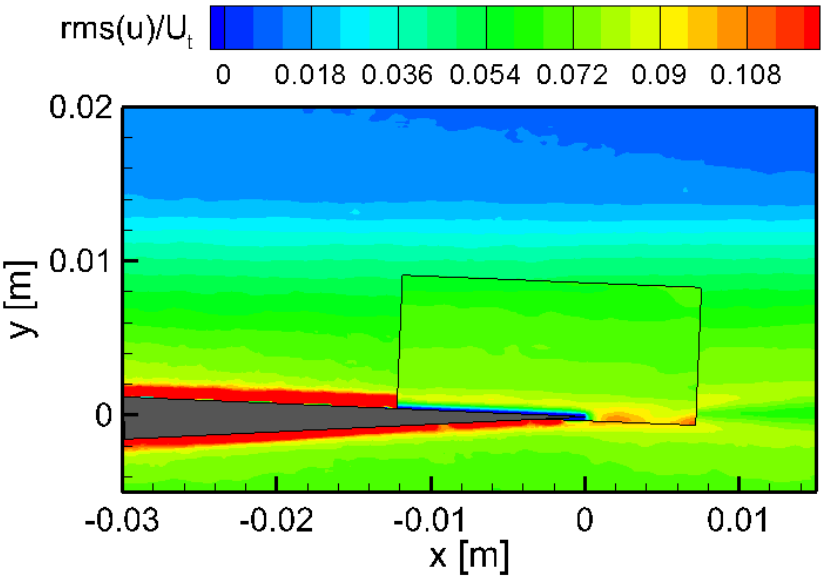

Figure 18. Contour plot of rms(u) normalized with tunnel velocity U_t, results in the boxed area were acquired by tomographic PIV.

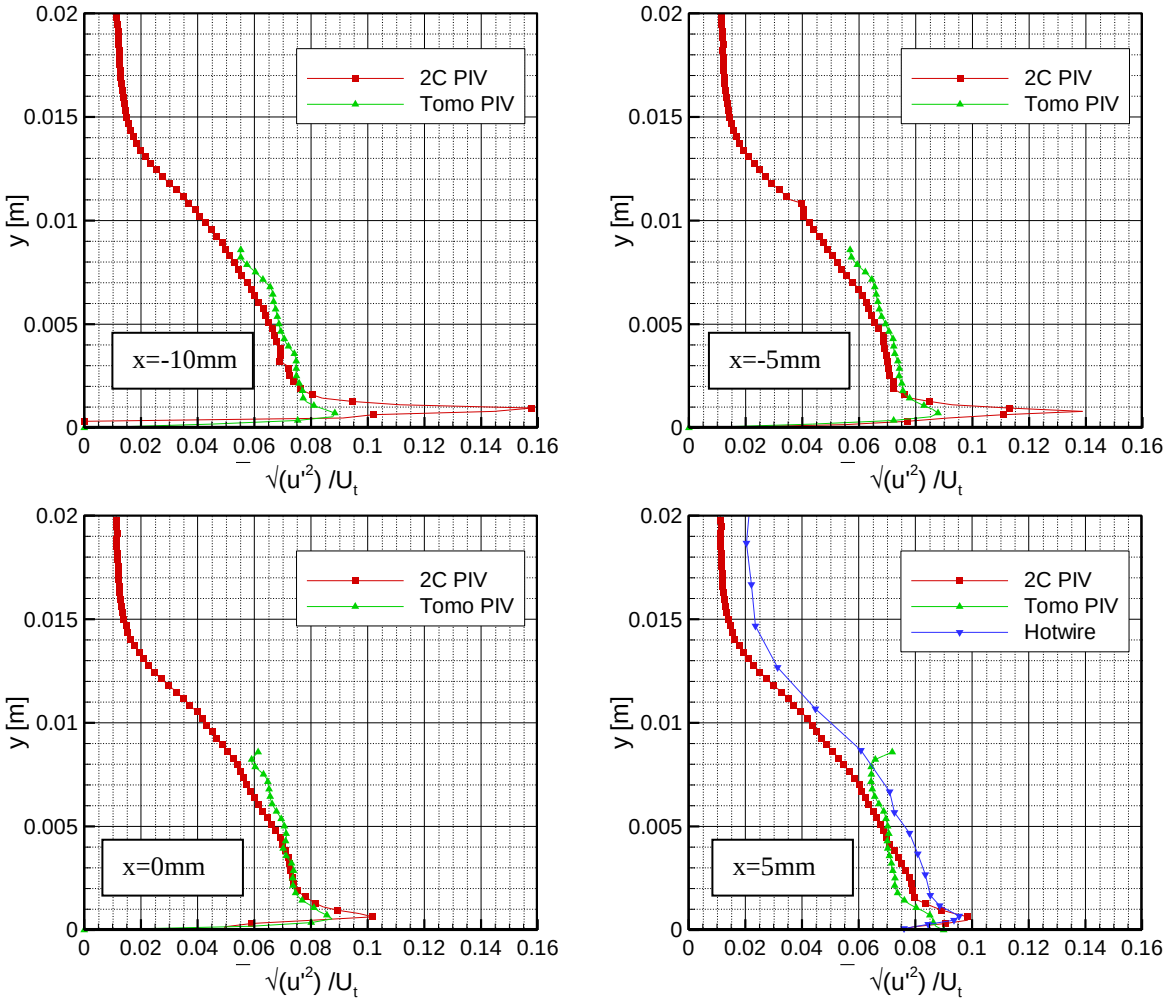

Figure 19. RMS profiles normalized with tunnel velocity U_t at x=-10mm, -5mm, 0mm and 5mm.

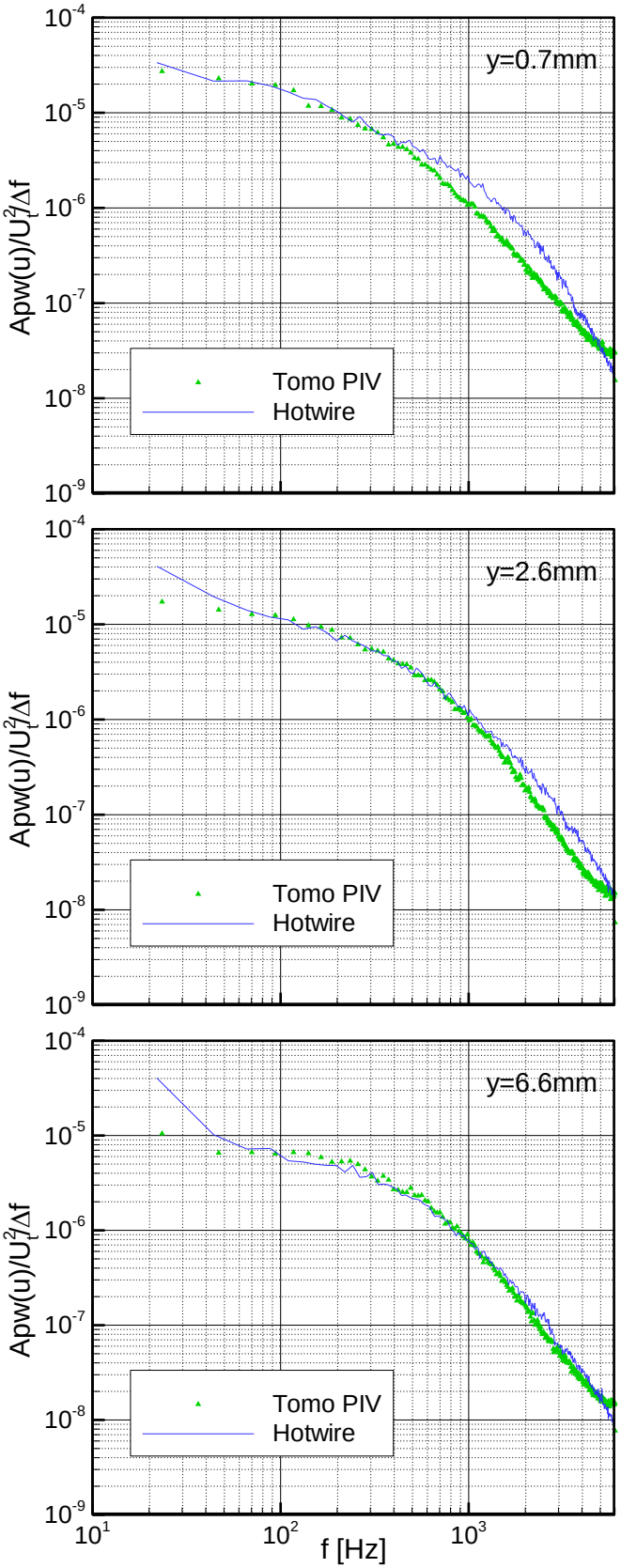

Figure 20. Hot-wire spectra compared to Tomographic PIV spectra at y=0.7mm, 2.6mm and 6.6mm.

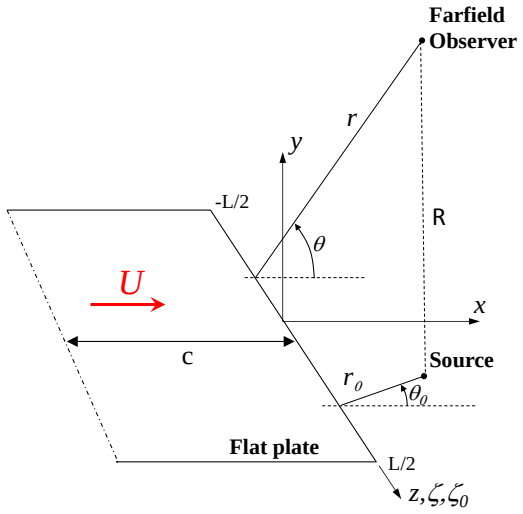

Figure 21. Coordinate and geometrical definitions

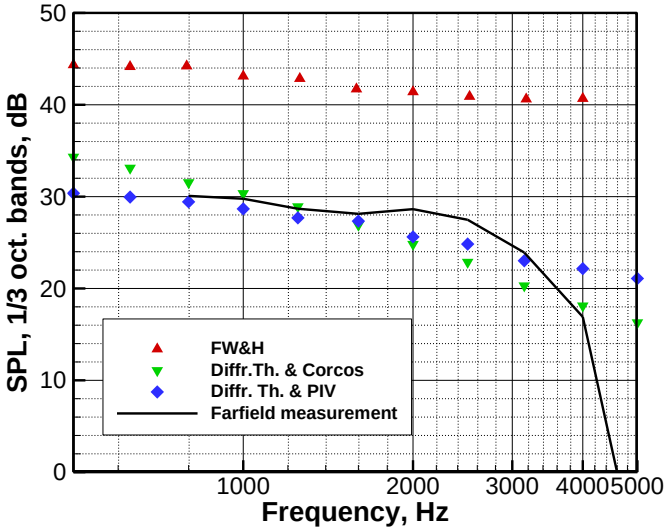

Figure 22. Sound power level (SPL at R=0.282) estimated from PIV measurements and comparison to acoustic measurements.